Evolution of the doping regimes in the Al-doped SnO_2 nanoparticles prepared by a polymer precursor method

2015 J. Phys.: Condens. Matter 27 095301

(http://iopscience.iop.org/0953-8984/27/9/095301)

IOP Publishing Journal of Physics: Condensed Matter
J. Phys.: Condens. Matter **27** (2015) 095301 (7pp) doi:10.1088/0953-8984/27/9/095301

Evolution of the doping regimes in the Al-doped SnO_2 nanoparticles prepared by a polymer precursor method

F H Aragón[1,2], J A H Coaquira[1], L Villegas-Lelovsky[1], S W da Silva[1], D F Cesar[3], L C C M Nagamine[4], R Cohen[4], E Menéndez-Proupin[5] and P C Morais[1,6]

[1] Instituto de Física, Universidade de Brasilia, Brasilia, DF 70910-900, Brazil
[2] Laboratorio de Física Aplicada, Centro de Desenvolvimento da Tecnologia Nuclear, Belo Horizonte, MG 3127-901, Brazil
[3] Departamento de Física, Universidade Federal de São Carlos, São Carlos 13.565-905, Brazil
[4] Instituto de Física, Universidade de São Paulo, SP 05508-090, Brazil
[5] Departamento de Física, Facultad de Ciencias, Universidad de Chile, Las Palmeras 3425, 780-0003 Ñuñoa, Santiago, Chile
[6] Huazhong University of Science and Technology, School of Automation, Wuhan 430074, People's Republic of China

E-mail: fermin964@hotmail.com

Received 27 October 2014, revised 14 January 2015
Accepted for publication 16 January 2015
Published 13 February 2015

Abstract

In this study, we report on the structural and hyperfine properties of Al-doped SnO_2 nanoparticles synthesized by a polymer precursor method. The x-ray diffraction data analysis carried out using the Rietveld refinement method shows the formation of only rutile-type structures in all samples, with decreasing of the mean crystallite size as the Al content. A systematic study of the unit cell, as well as the vicinity of the interstitial position show strong evidence of two doping regimes in the rutile-type structure of SnO_2. Below 7.5 mol% doping a dominant substitutional solution of Al^{+3} and Sn^{4+}-ions is determined. However, the occupation of both substitutional and interstitial sites is determined above 7.5 mol% doping. These findings are in good agreement with theoretical *ab initio* calculations.

Keywords: doped oxide semiconductor, substitutional position, interstitial position

(Some figures may appear in colour only in the online journal)

1. Introduction

Transparent conducting oxides such as SnO_2 have a great technological potential related to the ideal combination of electrical and optical properties. Since they have found many applications in technology, the SnO_2-based systems are extensively studied. Particularly, for gas sensing materials the sensitivity is strongly dependent upon the crystallite size and shape, inasmuch as this property is influenced by the surface-to-volume ratio in nanosized systems [1, 2]. High sensitivity of SnO_2 nanowires for NO_2 gas detection (which is one of the most dangerous air pollutants forming ozone acid rain) has been demonstrated in comparison with different types of sensors, including SnO_2 powder-based thin films, SnO_2 coating on carbon nanotubes, or single/multiple nanobelts [3]. The sensitivity enhancement was attributed to the high surface-to-volume ratio of the one-dimensional (1D) nanostructures. For this type of application, the electrical conductivity is a very important issue, as demonstrated by many studies focused on this subject. Unambiguously, the conduction mechanism of undoped SnO_2 is correlated with nonstoichiometry [4]. It can be explained by the fact that Sn-related ions have four valence electrons. Meanwhile, O ions are two-fold charged and any point defect at the particle surface such as oxygen vacancy (V_O), for instance, drives to have an excess of Sn-related ions and then the system shows *n*-type conductivity.

First-principles calculation suggested that V_O and the presence of interstitial tin ions (Sn_i) in SnO_2 can explain the occurrence of natural n-type carriers in this material [5]. On the other hand, the doping of the SnO_2 matrix with a specific element has allowed for the development of highly selective gas sensors [6]. Moreover, the doping provides desirable electrical, structural, optical and/or magnetic properties to the hosting compound. In this scenario, Maldonado *et al* [7] reported changes in the structural, electrical and electronic properties of the ZnO compound due to the Al-doping using a quantum-chemical approach based on the Hartree–Fock theory. According to the authors, the Al-doping generates a free electron in the conduction band due to the ionic substitution of Al^{3+} by Zn^{2+}. In particular, the substitution of Al^{3+} by Sn^{4+}-ions in the SnO_2 system creates oxygen vacancies due to the charge imbalance, generating free electrons in the conduction band. According to previous reports on Er-doped SnO_2 nanoparticles, synthesized by a polymeric precursor method, the lattice constants, Sn–O bond distances and bond angles change strongly, suggesting the substitutional solution of Er^{3+} and Sn^{4+}-ions in the SnO_2 matrix and the onset of oxygen vacancies for dopant contents up to 10 mol% [8]. Furthermore, Ahmed *et al* [9] claimed that the doping with Al can induce a change from a n-type to a p-type as the Al-content is increased in the Al-doped SnO_2 system. The latter effect opens up the possibility of combining two types of transparent conducting oxides while building a $p-n$ junction. However, evidence for the mechanism of doping, the places occupied by the Al atoms in the SnO_2 matrix and the sources for the change in carrier type in the Al-doped SnO_2 system remain unclear. In order to shed new light on these issues, we report herein a systematic study of the structural and hyperfine properties of Al-doped SnO_2 (SnO_2:Al^{3+}) nanoparticles synthesized by a polymer precursor method while varying the Al-content from 1.0 to 50.0 mol%. Moreover, first principles calculations were also carried out to validate and support our interpretation of the experimental results.

2. Experimental details

SnO_2:Al^{3+} nanoparticles with Al-content in the range from 1 to 50 mol% have been synthesized by a polymeric precursor method. A former solution was obtained by mixing nominal amounts of the tin precursor, tin citrate $Sn_2(C_6O_7H_4)\cdot H_2O$, previously obtained from $SnCl_2\cdot 2H_2O$, and the Al precursor $Al(NO_3)_3\cdot 9H_2O$. The amount of Al was controlled by using the Al/(Al + Sn) ratio. The resultant product was firstly calcinated at 400 °C for 4 h and, after grinding using an agate mortar, an additional calcination at 500 °C for 15 h has been done in order to warrant the phase formation and good crystallinity. Further preparation details are reported elsewhere [10, 11]. X-ray powder diffraction (XRD) patterns were obtained by using a commercial diffractometer with a Cu K_α radiation source. The lattice parameters as well as the average crystallite size were determined from the XRD data analysis using the Rietveld refinement method. The particle size and morphology have been determined by transmission electron microscopy (TEM) and high-resolution TEM micrographs. Mössbauer spectroscopy measurements were carried out using a $Ca^{119m}SnO_3$ radiation source. A natural Sn foil was used as the absorber for the calibration and the calibration error was estimated to be less than 0.5%. All spectra were recorded at room temperature and the isomer shift (IS) values were calculated with respect to $CaSnO_3$. The analysis of the spectra were obtained with a least-square fitting routine assuming a Lorentzian lineshape and considering the hyperfine splitting of $I = 3/2,\ 1/2$ nuclear levels in the usual way.

3. Calculation method

The first-principles calculations have been performed with the *ab initio* total-energy calculations using the well-established SIESTA (Spanish Initiative for Electronic Simulations with Thousands of Atoms code [12], which is based on the density functional theory (DFT). The exchange and correlation energies are treated as the standard Kohn–Sham self-consistent density functional method in the local density approximation (LDA), which is accurate enough to calculate structural properties. To study the effect of the Al-doping we have used a $2\times2\times2$ supercell, which contains 48 atoms ($Sn_{16}O_{32}$). The optimization of the unit cell volume (V) has been carried out following two steps: (i) computing the total energy (E) for several values of V, and (ii) fitting the E versus V in accordance with the Murnaghan's equation [13] given by:

$$E(V) = E_0 + \frac{B_0 V}{B_0'}\left(\left(\frac{V_0}{V}\right)^{B_0'}\frac{1}{B_0'-1}+1\right) - \frac{B_0 V}{B_0'-1} \qquad (1)$$

where E_0 is the total energy at the minimum, B_0 the bulk modulus and B_0' the pressure derivative of the bulk modulus at the equilibrium volume. After the fitting, the equilibrium volume (V_0) has been obtained.

4. Results and discussion

4.1. Structural and microscopic properties

The XRD patterns of the SnO_2:Al^{3+} nanoparticles have been refined by the Rietveld refinement method using the DBWS program [14]. Data analyis confirmsp that the reflections are consistent with the rutile-type crystalline structure and excluded the presence of additional crystalline or amorphous phases even for the highly doped samples (up to 50 mol%). The observed and calculated profiles of the XRD patterns are shown in figure 1(a). The presence of the rutile-type crystalline phase has been corroborated by Raman spectroscopy measurements (not shown here). Raman spectra of all Al-doped SnO_2 samples show vibrational modes which are consistent with only the rutile-type phase. Lattice parameters obtained for the undoped SnO_2 nanoparticles are $a = 4.7371$ Å and $c = 3.1866$ Å, which are in good agreement with standard data files of the bulk SnO_2 compound (ICSD 39173; ICDD-PDF card No. 41-1445). As observed in figure 1(a), the linewidth (FWHM) of the Bragg reflections shows an increasing tendency as the Al-content is increased. This finding has been attributed to the crystallite size reduction.

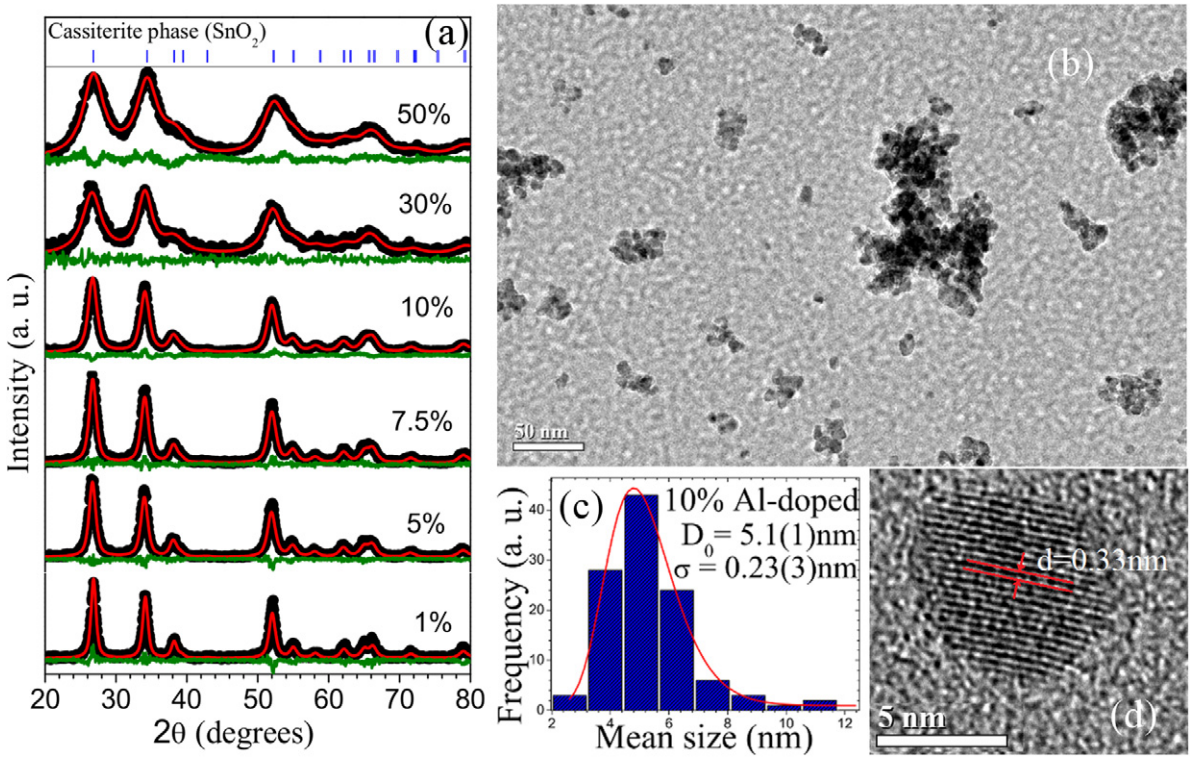

Figure 1. (*a*) X-ray diffraction (XRD) patterns of the Al-doped SnO_2 nanoparticles. The observed and calculated data are represented by symbols and solid lines, respectively. Differences between observed and calculated data are also shown. The blue lines in the top represent the expected position for the tetragonal SnO_2 rutile-type structure. (*b*) TEM image obtained for the 10 mol% Al-doped SnO_2 sample. (*c*) The histogram distribution of the particle size. The solid line represents the log-normal function. (*d*) High-resolution TEM image of the 10% Al doped sample, where the interplanar distance of 0.33 nm corresponds to the (1 1 0) planes of rutile-type structure.

In order to investigate the structural properties, the XRD peak shape has been modeled using the Thompson–Cox–Hastings pseudo–Voigt function, where L and G represent the Lorentzian and Gaussian functions, respectively, and η is a mixing parameter [15, 16]. The line broadening related to the instrumental contribution was corrected by adequately subtracting the linewidth of a standard sample (*Si* single crystal) from the linewidth of the studied samples. A list of structural parameters obtained from the Rietveld refinements is presented in table 1.

The mean crystallite size is estimated to be ∼11 nm for the undoped sample and this crystallite size shows a decreasing tendency as the Al-content is increased. This is an important effect of the doping, which has also been observed in Ni-, Fe- and Mg-doped SnO_2 nanoparticles [11, 17, 18]. In order to further corroborate the XRD results, TEM images have been obtained. Figure 1(*b*) shows a TEM image of the particle size for 10 mol% Al-doped sample. Several images were used to obtain a total of $N = 110$ particles sizes. Subsequently, a particle size histogram was mounted using the Sturges method. The bin-width (W) is obtained from the relation: $W = (D_{\max} - D_{\min})/k$, where $k = 1 + 3.322\log(N)$. The histogram is fairly well modeled by a log-normal distribution, as shown in figure 1(*c*). A mean particle size of 5.2 nm is estimated by using the relation $< D >= D_0 \exp(\sigma^2/2)$, where D_0 is the median size and σ is the polydispersity parameter. The mean size determined from the TEM micrographs is in good agreement with the mean crystalline size determined from the XRD data analysis. Figure 1(*d*) shows the high resolution TEM (HRTEM) image of the 10 mol% Al-doped sample. The measured interplanar distance is $d = 0.33$ nm, which corresponds to the orientation of the (1 1 0) planes of the tetragonal structure of SnO_2.

Both lattice parameters (a and c) show a decreasing tendency with the Al-content nearly with the same rate up to 7.5 mol%. Above that Al-content the lattice parameter c is still showing a decreasing tendency, although with a lower rate; meanwhile the parameter a shows an opposite trend, increasing above 7.5 mol%, as shown in figure 2(*a*). Moreover, the c/a ratio shows a nearly linear decrease with the Al-content (x) (see table 1), suggesting an anisotropic compression of the unit cell along the c axis, which becomes stronger as the the Al-content is increased. Finally, the unit cell volume (V) shows a linear decrease ($\mathrm{d}V/\mathrm{d}x \sim -6.00$ Å^3) with the Al-content up to 7.5 mol% (see figure 2(*b*)). Above that content the rate of decrease of V change to $\mathrm{d}V/\mathrm{d}x \sim 1.15$Å^3 as x increases, reflecting the Al-content dependence of the lattice parameters. These results strongly suggest that below 7.5 mol% of Al-doping a substitutional solution (solid solution) regime must dominate the doping process. In that region, both lattice parameters are affected similarly and the observed reduction is due to the substitution of the Sn^{4+}-ions (ionic radius of 0.71Å) by the smaller Al^{3+}-ions (ionic radius of 0.51Å). However, above 7.5 mol% the substitutional solution regime must coexist with the entrance of Al^{3+}-ions into interstitial sites of the rutile-type structure. This finding is consistent

Table 1. List of the parameters obtained from the Rietveld refinement of the XRD data for the SnO_2:Al^{3+} nanoparticles. The quality of the refinement is represented by the S factor ($S = R_{wp}/R_{exp}$).

Al-content (mol%)	Mean Crystallite Size (nm)	a (Å)	c (Å)	u	c/a	S (%)
0.0	11.0(5)	4.7371	3.1866	0.3094	0.6727	1.17
1.0	9.6(5)	4.7385	3.1853	0.3043	0.6722	1.27
2.5	7.5(5)	4.7354	3.1844	0.3042	0.6725	1.34
5.0	6.2(5)	4.7310	3.1805	0.3026	0.6723	1.20
7.5	5.8(5)	4.7310	3.1788	0.3024	0.6719	1.15
10.0	5.6(5)	4.7314	3.1738	0.2997	0.6708	1.96
30.0	2.5(5)	4.7330	3.1654	0.2922	0.6688	1.40
50.0	1.8(5)	4.7345	3.1491	0.2797	0.6651	1.74

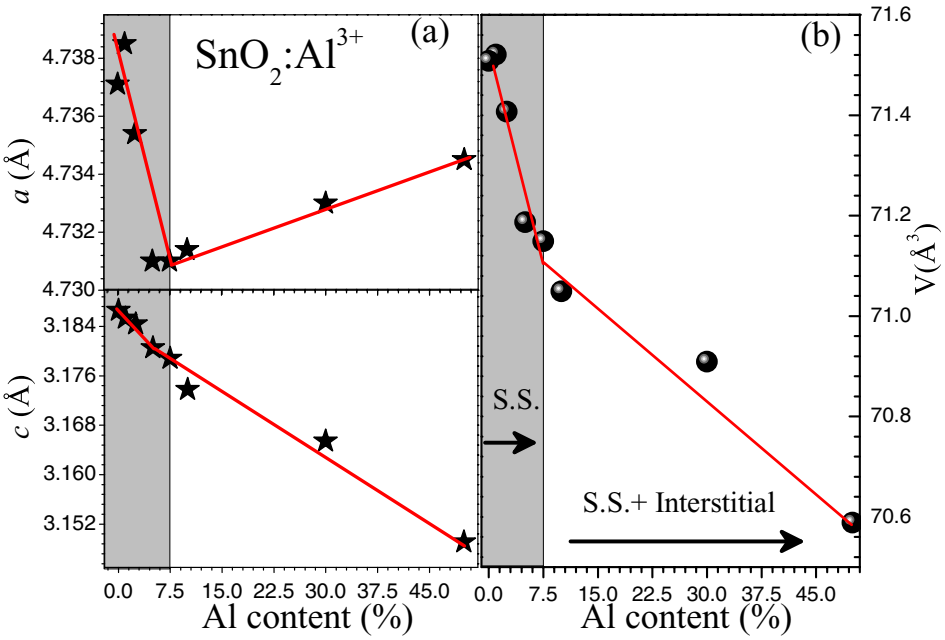

Figure 2. (a) Plot of the lattice parameters (a and c) and (b) unit cell volume (V) as a function of the Al-content in the SnO_2:Al^{3+} nanoparticles. (The solid lines are drawn to guide the eyes).

with theoretical studies, which indicate that the Al^{3+}-ions can enter into the SnO_2 matrix and they can occupy substitutional or interstitial sites of the SnO_2 matrix in order to compensate the charge imbalance [19]. According to the literature [19], the interstitial sites allowed for cation doping occupancy in the rutile-type structure are located at (0, 0.5, 0.5), which is the center of an unoccupied oxygen octahedron (see figure 3). The entrance of Al^{3+}-ions into those interstitial sites can explain the increasing tendency of the lattice parameter a above $x > 7.5$ mol%, since a smaller value of a is expected for unoccupied interstitial sites. On the other hand, the disturbance originated by the entry of Al^{3+}-ions is also evidenced by the decreasing tendency showed by the internal parameter u (see table 1). In order to assess further information the possible changes in the Sn–O–Al angles and O–Al bond distances structural parameters around the interstitial site likely occupied by Al^{3+}-ions were calculated.

As shown in figure 3, the interatomic distance between the central Al^{3+}-ion and the oxygen ions forming the octahedron is represented by just two distances: the apical distance (d_1) between the central Al^{3+}-ion and one of the oxygen ions (O_1) located at (u, u, 0) and the basal plane distance (d_2) between the central Al^{3+}-ion and one of the oxygen ions of the basal plane (O_2), which is located at ($0.5 - u$, $0.5 + u$, 0.5). These two distances are calculated by using the refined parameters a, c and u. According to the crystal structure, the d_1 and d_2 distances are given by:

$$d_1 = au\hat{i} + a(u - 0.5)\hat{j} + 0c\hat{k} \tag{2}$$

and

$$d_2 = a(0.5 - u)\hat{i} + au\hat{j} + 0.5c\hat{k} \tag{3}$$

Here, $\hat{i}$, $\hat{j}$ and $\hat{k}$ are the unit vectors along the x-axis, y-axis and z-axis, respectively. The basal plane angle (θ) is given by:

$$\cos(\theta) = [a^2(1 - 4u + 8u^2) - 1] / [c^2 + 4a^2(0.5 - u)^2 + 4a^2u^2] \tag{4}$$

Figure 4 shows the Al-content dependence of d_1, d_2, and θ. The values of d_1 and d_2 for the undoped sample indicate that the apical distance is smaller than the basal plane distance. Both Al–O bond distances (d_1, d_2) show a rapid decrease as the Al-content is increased up to 7.5 mol%. In this region, the

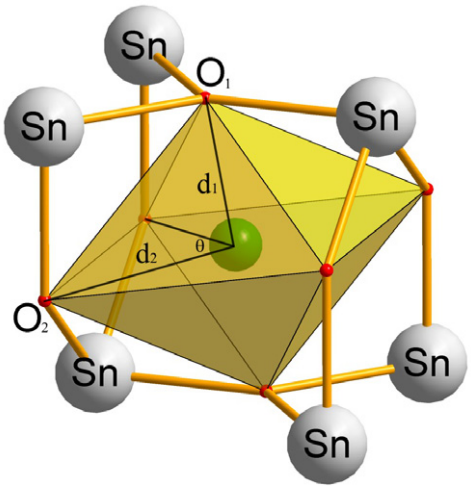

Figure 3. Schematic representation of the unoccupied oxygen octahedron around the interstitial site. The interstitial position is represented by the green sphere. The apical distance (d_1), the basal plane distance (d_2), and the angle θ are indicated.

angle θ shows an increasing tendency which indicates that the symmetry of the octahedron becomes less distorted with the entrance of the Al^{3+}-ions substituting the Sn^{4+}-ions. Above this content the rate of decreasing of both distances is reduced. Meanwhile, the angle θ shows a small increasing rate with the Al-content. The change in the rate at $x \sim 7.5$ mol% has been attributed to the onset of the entrance of Al^{3+}-ions into interstitial sites above $x > 7.5$ mol%.

4.2. Hyperfine properties

Room-temperature Mössbauer spectroscopy (MS) data were recorded out for all of the studied samples. Figure 5 shows the MS spectra of samples doped with 1.0, 7.5 and 50.0 mol%. Within the experimental resolution the preliminary analysis excluded the presence of magnetic interactions (sextets) and it indicates that the whole set of samples is well resolved by considering quadrupole electric interactions (doublets). Due to the crystal symmetry there is only one site for Sn^{4+}-ions, leading to only one expected doublet for bulk SnO_2. However, the fit of the Mössbauer data considering only one doublet provides a linewidth of $\sim$2.0 mm s^{-1}. This linewidth is larger than the expected for bulk SnO_2 and suggests the occurrence of several geometrical or electronic surroundings near to the Sn nuclei, which can produce a wide distribution of electric quadrupole splitting (QS). In order to build a better physical picture of the system the MS data were fitted with a distribution of QS's using the NORMOS-DIST program [20]. The fitted spectra and their QS histograms are shown in figure 5. The QS's histograms show asymmetrical shapes with a broad peak at the lower part of the QS's centered around 0.9 mm s^{-1}. The contributions coming from the high-QS region of the histogram can be attributed to the several non-equivalent surroundings created by the entrance of the doping ions. Even more interesting is the result obtained from the evolution of the isomer shift (IS) as a function of the Al-content. It is worth mentioning that despite the small change in the IS values and their narrow error bars determined from the fit, we showed in a previous

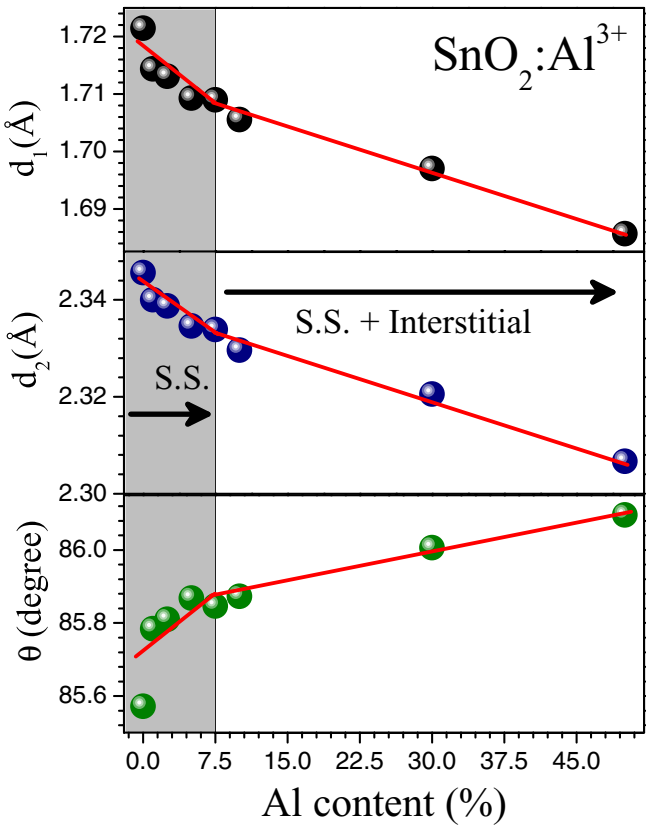

Figure 4. Evolution of the apical distance (d_1), the basal plane distance (d_2) and the angle θ in the basal with the Al-content in the Al-doped SnO_2 nanoparticles. (The solid lines are drawn to guide the eyes).

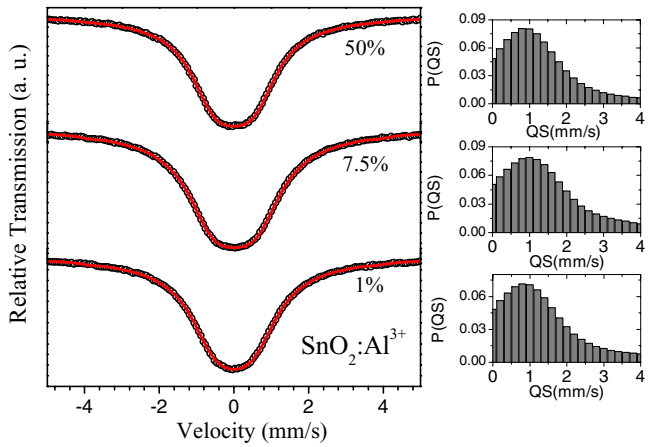

Figure 5. Room-temperature Mössbauer spectra of the Al-doped SnO_2 nanoparticles. Symbols represent the experimental data and solid lines represent the fit to a distribution of QS. The histogram distributions of QS's are also shown.

study [15] a highly reproducible qualitative behavior of IS. As shown in figure 6, two distinct behaviors can be observed.

For Al-content up to 7.5 mol% a linear increase of the IS with a rate of $dIS/dx \sim 0.46$ mm s^{-1} is determined. Above that Al-content an opposite tendency of the IS with a rate of $dIS/dx \sim -0.03$ mm s^{-1} is determined. The linear increase of the IS observed for the low Al-content region has been assigned to the substitution of Al^{3+} by Sn^{4+}-ions in the SnO_2

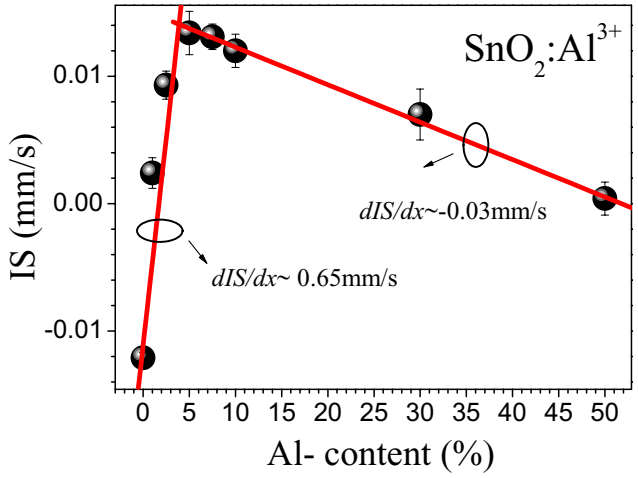

Figure 6. Dependence of the isomer shift (IS) on the Al-content. The solid spheres represent the experimental data and the solid lines represent the linear fits.

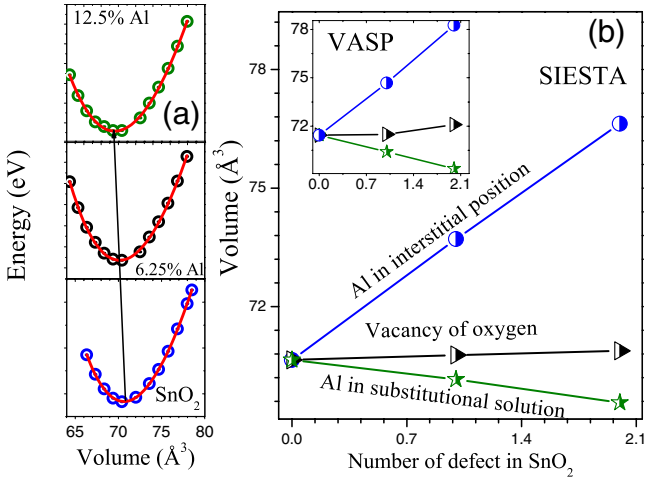

Figure 7. (a) Plot of the total energy calculated by DFT for the undoped and the Al-doped (6.25 and 12.5%) SnO_2 supercell as a function of the unit cell volume (V). The red line represents the fit using the Murnaghan relation (equation (1)). (b) Evolution of the unit cell volume with the number of Al^{3+}-ions occupying substitutional or interstitial sites and oxygen vacancies (number of defects in SnO_2) obtained by using the SIESTA method. The inset shows the theoretical calculations obtained by using the VASP method.

matrix, in agreement with the XRD results. The substitutional doping must provide free electrons to the conduction band arising from the generation of oxygen vacancies in order to compensate for the charge imbalance. As those electrons are expected to be of s-type character they contribute directly to the increase of the IS. Similar increasing tendency of IS when the dopant content is increased has been reported for other lower valence dopants (lower than 4+) [8]. However, the drastic change in the rate of the IS observed above 7.5 mol% of Al-content must be the result of contribution coming from both the interstitial and substitutional sites occupations, as suggested by the XRD results. It means that the decreasing behavior of the IS as the Al-content is increased above 7.5 mol% suggests that the occupancy of the interstitial sites reduces the generation of the oxygen vacancies, which provides s-type electrons to the system. Instead, the occupancy of the interstitial sites can produce a defect inside the band gap near to the top of the valence band, thus providing holes to the system. The latter result is in agreement with the results reported by Mehdi *et al* for Al-doped SnO_2 films [21]. The authors determined a change in charge type from n-type to p-type above 8 mol% of Al-content which was ascribed to the extra hole generated as the Al-content was increased.

4.3. Theoretical study

In order to give support to the experimental results related to the occupancy of the Al^{3+}-ions in the Al-doped SnO_2 system, the structural parameters of the rutile-type structure have been determined by first principles calculations. The Al-dopant ions have been located in two different ways: (i) as a substitutional solution ($Sn_{16-x}Al_xO_{32}$), when the Sn^{4+}-ions are replaced by the Al^{3+}-ions, (ii) in interstitial sites ($Sn_{16}Al_xO_{32}$), when the Al^{3+}-ions are located at the cation-preferred octahedral interstitial sites (shown in figure 3). Figure 7(a) shows the energy (E) versus volume (V) plot for the undoped, 6.25 mol%, and 12.5 mol% of Al-content. The fit of the calculated data points has been carried out in accordance with the Murnaghan's relation (equation (1)). Results indicate that for the undoped system the energy shows a minimum for a volume of 70.7 ± 0.1 Å^3, which is in good agreement with the experimental value of 71.5 Å^3 and with a reported value obtained from theoretical calculation [5]. Furthermore, the bulk modulus value found in our calculation (=267±12 GPa) is in agreement with experimental values reported in the literature (218–270 GPa) [22, 23].

As the Al-content is increased the unit cell volume shows a linear decreasing tendency, as shown in figure 7(b). For the Al-content region below 7.5 mol% the volume rate of $dV/dx \sim -6.00$ Å^3 obtained experimentally (see figure 2(b)) is in good agreement with the rate determined from our theoretical calculation ($dV/dx_{Sn} = -8.7 \pm 0.4$ Å^3, volume rate due to the Al^{3+}-ions occupying substitutional site). This result corroborates the assumption that at low Al-content the doping regime is governed by the substitution of Sn^{4+} by Al^{3+}-ions in the SnO_2 matrix. Above 7.5 mol%, the experimental volume rate becomes lower than the calculated one. Interestingly, it is determined that the occupation of the interstitial sites for the Al^{3+}-ions provides an increase in the unit cell volume, as shown in figure 7(b). This finding has been assigned to the strong electrostatic interaction between an Al^{3+}-ion and the nearest neighbor Sn^{4+}-ion located in the octahedron of the substitutional site which shares a common face with the interstitial octahedron occupied by the dopant. The effect of the oxygen vacancies on the unit cell volume has been tested and the results indicate no significant variation. This result shows that the oxygen vacancies cannot be responsible for the variation of the unit cell volume, as observed experimentally. On the other hand, in order to corroborate these effects, we have performed the same theoretical calculation using the Viena *ab-initio* simulate package (VASP) method. The obtained results are consistent with the results obtained by using the SIESTA method. Since the contribution of both substitutional and

interstitial sites occupancy of the dopant cation is expected for dopant content above 7.5 mol%, the experimental volume rate, dV/dx, can be given by:

$$\frac{dV}{dx} = y\frac{dV}{dx_{Sn}} + (1-y)\frac{dV}{dx_{Int}} \quad (5)$$

where dV/dx_{Int} is the volume rate due to the Al^{3+}-ions occupying interstitial sites, and y represents the fraction of the substitutional occupancy. Using the $dV/dx_{Sn} = -8.7 \pm 4$ Å^3, valid for the low Al-content region, and the volume rate of interstitial occupancy of $dV/dx_{Int} = 23.9 \pm 3$ Å^3, a fraction of substitutional occupancy of ~0.77 is determined from our data.

5. Conclusions

Al-doped SnO_2 nanoparticles with a rutile-type structure have been successfully synthesized by a polymer precursor method. The structural characterization of the Al-doped SnO_2 nanoparticles shows a strong dependency of the lattice parameters on the Al-content. A decreasing tendency of unit cell volume (V) as the Al-content is increased up to 7.5 mol% has been related to the substitutional solution of the Al^{3+} and Sn^{4+}-ions in the SnO_2 matrix. Above that Al-content, the decelerated rate of V has been found to be consistent with the occurrence of both substitutional and interstitial sites occupancy. Moreover, the isomer shift (IS) values determined from the Mössbauer spectra as a function of the Al-content shows two remarkable trends: a linear increase of IS when the Al-content increases up to 7.5 mol% and the opposite tendency of IS for higher Al-doping. These results are found to support the XRD results. First-principles calculations show that the dopant occupation of substitutional sites drives to the decrease of the unit cell volume, whereas the occupation of interstitial sites drives to the increase of the V. Those calculations are found to be consistent with the experimental results obtained for the Al-doped SnO_2 nanoparticles.

Acknowledgments

The authors thank the Brazilian agencies CAPES, CNPq, FAPESP (Proc: 2011/50556-0 and 2011/17944-6) and FAPDF for the financial support.

References

[1] Ponzoni A, Comini E, Sberveglier G, Zhou J, Deng S Z, Xu N S, Ding Y and Wang Z L 2006 *Appl. Phys. Lett.* **88** 203101
[2] Qi Q, Zhang T, Liu L and Zheng X 2009 *Sensors Actuators* B **137** 471
[3] Choi Y-J, Hwang I-S, Park J-G, Choi K J, Park J-H and Lee J-H 2008 *Nanotechnology* **19** 095508
[4] Stjerna B, Granqviest C G, Seidel A and Häggström L 1990 *J. Appl. Phys.* **68** 6241
[5] Kiliç Ç and Zunger A 2002 *Phys. Rev. Lett.* **88** 095501
[6] Jia L, Cai W and Wang H 2010 *Appl. Phys. Lett.* **96** 103
[7] Maldonado F and Stashans A 2010 *J. Phys. Chem. Solids* **71** 784
[8] Aragón F H, Coaquira J A H, Hidalgo P, Cohen R, Nagamine L C C M, da Silva S W, Morais P C and Brito H F 2013 *J. Nanopart. Res.* **15** 1343
[9] Ahmed Sk F, Khan S, Ghosh P K, Mitra M K and Chattopadhyay K K 2006 *J. Sol-Gel Sci. Technol.* **39** 241
[10] Aragón F H, Coaquira J A H, Hidalgo P, Brito S L M, Gouvêa D and Castro R H R 2010 *J. Non-Cryst. Solids* **356** 2960
[11] Hidalgo P, Castro R H R, Coelho A C V and Gouvêa D 2005 *Chem. Mater.* **17** 4149
[12] Soler J M, Artacho E, Gale J, Garcia A, Junquera J, Ordejón P and Sánchez-Portal D 2002 *J. Phys.: Condens. Matter* **14** 2745
[13] Murnaghan F D 1944 *Proc. Natl Acad. Sci. USA* **30** 244
[14] Young R A, Larson A C and Paiva-Santos C O 1998 *User's Guide to Program DBWS9807* (Atlanta, GA: School of Physics, Georgia Institute of Technology)
[15] Aragón F H, Cohen R, Coaquira J A H, Barros G V, Hidalgo P, Nagamine L C C M and Gouvêa D 2011 *Hyperfine Interact.* **202** 73
[16] Paiva C O, Cavalheiro A A, Cilense M A, Varela J A, Silva M T and Mascarenhas Y P 2001 *Adv. X-Ray Anal.* **44** 38
[17] Castro R H R, Hidalgo P, Coaquira J A H, Bettini J, Zanchet D and Gouvêa D 2005 *Eur. J. Inorg. Chem.* **11** 2134
[18] Pereira G J, Castro R H R, Hidalgo P and Gouvêa D 2002 *Appl. Surf. Sci.* **195** 277
[19] Freeman C M and Catlow C R A 1990 *J. Solid State Chem.* **85** 65
[20] Brand R A 1987 *Nucl. Instrum. Methods Phys. Res.* B **28** 398
[21] Mehdi M, Mohagheghi B and Saremi M S 2004 *J. Phys. D: Appl. Phys.* **37** 1248
[22] Camargo A C, Igualada J A, Beltr A, Llusar R, Longo E and Andrés J 1996 *Chem. Phys.* **212** 381
[23] Jiang J Z, Gerward L and Olsen J S 2001 *Scr. Mater.* **44** 1983